Adaptive phase field simulation of dendritic growth in a forced flow at various supercoolings

C. W. Lan,* C. M. Hsu, C. C. Liu, and Y. C. Chang
Department of Chemical Engineering, National Taiwan University, Taipei 10617, Taiwan, Republic of China
(Received 30 November 2001; published 13 June 2002)

An efficient finite volume method is developed for the phase-field simulation of two-dimensional dendritic growth in a forced flow at various supercoolings. The adaptive nature of the method allows the dendrite in a large domain to evolve secondary structures, even at low supercoolings. In addition to good agreement with previous calculations on the tip shape and speed, the effects of forced flow at various supercoolings are investigated and compared with the Oseen-Ivantsov solution and good agreement is found. The steady dendrite shape in all cases continues to have a self-affine nature and the invariant scaling parameters are in good agreement with the estimation.

DOI: 10.1103/PhysRevE.65.061601 PACS number(s): 68.70.+w, 81.30.Fb

I. INTRODUCTION

The development of microstructures is important in solidification processing, but it is a complicated physical process. For a nucleus in a supercooled environment, as the thermodynamic driving force overcomes the kinetic barrier, it starts growth and the morphology develops. Without the kinetic effect and interfacial energy, the growth defines the well-known Stefan problem for a diffusive growth. Ivantsov [1] first obtained a simple exact solution, i.e., $VR=f(\Delta)$, and demonstrated that the dendrite shape remains to be parabolic; V is the growth rate, R the tip radius, and Δ the dimensionless supercooling; $\Delta=(T-T_m)/(\Delta H/C_p)$, where T is the temperature, T_m the melting point, ΔH the heat of fusion, and C_p the specific heat. The development of solvability theory [2,3] has also led to further understanding of the growth operating state, where the anisotropic surface energy selects uniquely the tip velocity and shape. The scaling parameter $\sigma=2\alpha d_0/VR^2$ depends only on the strength of the anisotropy ε; α is the thermal diffusivity and d_0 the capillary length. The theory has been validated recently by phase-field simulation. The extension of the microsovability theory for a parabolic dendrite under a uniform flow in two dimensions (2D) was made by Bouissou and Pelce [4]. However, the details of the structure development of dendrite growth require a global model and this renders the numerical solution of a complete time-dependent Stefan problem coupled with the fluid flow. Solving the problem using front tracking is extremely challenging due to the large deformation of the dendrite shape.

With the progress of phase-field simulation [5–8], the simulation of dendritic growth has been greatly simplified. The phase field introduces a continuous phase-field variable $\phi(\mathbf{r})$ to describe the interface through a rapid transition of the function. Nevertheless, the phase-field simulation is not exactly the same as the front tracking unless the sharp interface limit, where the interface thickness is much smaller than the capillary one, can be approached. Karma and Rappel [5] provided simple criteria of choosing parameters such that the sharp interface limit can be released to the order of the capillary length. Moreover, the solvability theory has been validated by phase-field simulations in 2D and 3D, but only focused on the purely diffusive regime. For the situation under a forced flow, Tong, Beckermann, and Karma [9] made the first attempt to validate the Oseen-Ivantsov solution proposed by Bouissou and Pelce [4] for a large supercooling ($\Delta=-0.55$). Their calculations agree well with the Oseen-Ivantsov solution, but, interestingly, only if the dendrite tip radius is obtained from a parabolic function fitting the overall dendrite head. Their selection parameter depends weakly on the flow rate. Some experimental works [10–12] have also been proposed, but there is a lack of consensus in comparing theory and simulation.

Although the work by Tong, Beckermann, and Karma [9] has been a great success in validating the theory, their calculations are valid only for high supercoolings due to the use of a structured mesh in a small domain; the maximum domain size in their calculations was only $1024\times2048(\Delta x^2_{\min})$. As they mentioned, the simulation for low supercoolings, higher flow velocities, and in 3D remain a great challenge for the future. At a low supercooling (e.g., $\Delta=-0.1$), the dendrite tip growth rate is small (small growth Peclect number) and it takes a long time to reach a steady state. To avoid the far field being affected, the domain size for simulation needs to be increased dramatically. To overcome this, an adaptive approach is necessary. Provatas, Goldenfield, and Dantzig [6] proposed an efficient adaptive finite element method for simulation, and their domain size was up to $102\,400\times51\,200$, where the ratio of the largest to smallest cell size was 2^{17}. More importantly, their computing cost scales with the domain size (L^2). By doing so, they have found a small difference in the tip velocity with the theory, and the main reason is believed to be the effect of side arms. If the side-arm effect is suppressed, the agreement between computation and theory is improved. Still, for $\Delta=-0.1$, their tip velocity did not reach a steady state even after an extremely long time. Again, their calculations did not consider melt flow. Adaptive meshes were considered by Tonhardt and Amberg [13] as well. However, they considered a shear flow passing a seed on a wall and thus the comparison with theory was not possible. In addition, the side branching induced by the thermal noises due to the convection at low supercooling can

*Corresponding author. FAX: 886-2-2363-3917. Email address: cwlan@ccms.ntu.edu.tw

only be simulated by the adaptive mesh. The development of the side branches also provides the foundation for theory development and better understanding the physics.

In this study, we present an efficient phase-field simulation based on an adaptive finite volume method. Since an extremely large domain ($204\,800\times 102\,400$) and cell-size ratio (up to 2^{14-18}) are used and the computational cost is optimum, scaling linearly with the domain size, we are able to simulate the dendritic growth at low supercoolings in a forced flow, even at high flow velocities. This opens an additional window for the realistic simulation of dendritic growth and makes the comparison with the theory possible. Our domain size is greater than that reported by Provatas, Goldenfield, and Dantzig [6] and the flow velocities are larger than that used by Tong, Beckermann, and Karma [9], and this is not an upper limit. All the calculations are performed efficiently in a personal computer (Pentium-III/800 with 512 Mbyte SRAM) and the simulation approach can be extended to 3D easily.

In the following section, the model used is described briefly. The numerical method, i.e., adaptive finite volume method, for solving the model is introduced in Sec. III. Section IV is devoted to results and discussion, where benchmark comparisons with previous calculations are presented in details. Furthermore, the validation of the Oseen-Ivontsov solution at various supercoolings will be discussed. Finally, the self-affine nature of the steady growth is presented before the conclusion is made.

II. MATHEMATICAL FORMULATION

For comparison purposes, the dendritic growth is simulated using a phase-field model employed in [5]. The temperature is rescaled to $\theta=C_p(T-T_m)/\Delta H$, where C_p is the specific heat of the solid. The phase-field variable ϕ is set to 1 in the solid, -1 in melt, and 0 at the interface. The time t is rescaled by τ_0, which characterizes atomic movement, the length is rescaled by w_0, which characterizes the interface thickness, and the velocity is rescaled by α/w_0, where α is the dimensional thermal diffusivity. The energy and phase-field equations can be written as the following, respectively:

$$\frac{\partial\theta}{\partial t}+D\boldsymbol{\nabla}\cdot(\boldsymbol{\nu}\theta)=D\nabla^2\theta+\frac{1}{2}\frac{\partial\phi}{\partial t}, \tag{1}$$

$$\begin{aligned}A(\mathbf{n})^2\frac{\partial\phi}{\partial t}=&\boldsymbol{\nabla}\cdot[A(\mathbf{n})^2\boldsymbol{\nabla}\phi]+[\phi-\lambda\theta(1-\phi^2)](1-\phi^2)\\&+\frac{\partial}{\partial x}\left(|\boldsymbol{\nabla}\phi|^2A(\mathbf{n})\frac{\partial A(\mathbf{n})}{\partial\phi_{,x}}\right)\\&+\frac{\partial}{\partial y}\left(|\boldsymbol{\nabla}\phi|^2A(\mathbf{n})\frac{\partial A(\mathbf{n})}{\partial\phi_{,y}}\right),\end{aligned} \tag{2}$$

where D is the dimensionless thermal diffusivity ($D=\alpha\tau_0/w_0^2$) and $\boldsymbol{\nu}$ is the velocity, and for the growth of a dendrite having fourfold symmetry, such as succinonitrile (SCN),

$$A(\mathbf{n})=(1-3\varepsilon)\left[1+\frac{4\varepsilon}{1-3\varepsilon}\frac{(\phi_{,x})^4+(\phi_{,y})^4}{|\boldsymbol{\nabla}\phi|^4}\right], \tag{3}$$

where $\phi_{,x}$ and $\phi_{,y}$ represent $\partial\phi/\partial x$ and $\partial\phi/\partial y$, respectively, and ε is the anisotropy strength of surface energy. In addition, $\lambda=w_0a_1/d_0$ and $\tau_0=w_0^3a_1a_2/d_0\alpha+w_0^2\beta_0/d_0$; $a_1=0.8839$ and $a_2=0.6267$ [5,6]. In the above formulation, as discussed in [5], the kinetic effect can be neglected and this is realistic for low supercoolings. The calculation of the velocity requires the treatment of two-phase flow at the interface, and the model proposed by Beckermann *et al.* [14] is also adopted here. The conservation equations for mass and momentum are as follows, respectively:

$$\boldsymbol{\nabla}\cdot\boldsymbol{\nu}=0, \tag{4}$$

$$\frac{1}{D}\frac{\partial\boldsymbol{\nu}}{\partial t}+\boldsymbol{\nabla}\cdot(\boldsymbol{\nu}\boldsymbol{\nu})=\mathrm{Pr}\nabla^2\boldsymbol{\nu}-\nabla P+\mathbf{F}, \tag{5}$$

where $\mathrm{Pr}=\nu/\alpha$ is the Prandtl number and $\mathbf{F}$ accounts for the dissipative force between the two phases. In this study, $\mathrm{Pr}=23.1$ is used, which is about the value for succinonitrile. Also, the dimensionless pressure P has been rescaled by $\rho\alpha^2/w_0^2$, where ρ is the melt density; here, the melt and solid densities are assumed to be the same. The interactive force $\mathbf{F}=-0.5C\mathrm{Pr}[(\phi+1)/w_0]^2\boldsymbol{\nu}$, where C is an empirical constant. Beckermann *et al.* [14] used the analytical result of the Poiseuille flow between two plates to fit the model and got $C=2.757$. In this study, we mainly focus on the dendritic growth in a uniform forced flow. In order to compare with the theory and previous calculations, the buoyancy convection due to gravity is neglected, even though it can be added easily in the source term of the momentum equation. The boundary conditions are straightforward for the above equations. The far field temperature is set at the supercooling one and the velocity is determined by the stress-free condition. The inlet velocity is given to be U and the outflow boundary condition is set by the overall mass balance, while the melt is incompressible. The pressure at the boundary is then obtained by linear extrapolation from the interior points.

III. ADAPTIVE FINITE VOLUME METHOD

In order to have a large domain for calculation, while keeping the cells near the interface small enough, adaptive mesh refinement (AMR) is necessary. For simplicity, we have adopted a simple way to carry out refinement using quadrilateral cells. A sample mesh is shown in Fig. 1(a), where two local details are illustrated. The typical cell is shown in Fig. 1(b). For the refinement, the parent cell is subdivided into four daughter cells, while for coarsening, the daughter cells are deleted. Constructing the data structure is straightforward by using pointers and derived data types of FORTRAN90. A detailed description of the adaptive data structure and a sample program can be found elsewhere [15]. Before applying the finite volume approximation, the above conservation equations can be written with the following form:

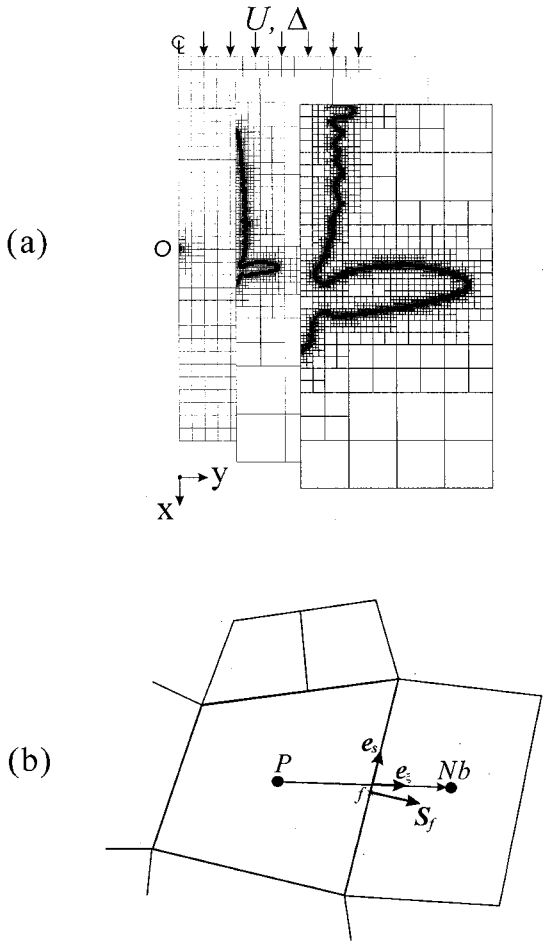

FIG. 1. (a) Adaptive mesh for dendritic growth in a forced flow; (b) a sample finite volume cell.

$$a_\varphi \frac{\partial \varphi}{\partial t} + \nabla \cdot (b_\varphi \boldsymbol{\nu} \varphi) = \nabla \cdot \Gamma_\varphi \nabla \varphi + B_\varphi , \tag{6}$$

where φ represents the conservation variable, and the corresponding coefficients are summarized in Table I. Then, for a control cell, with an arbitrary number of neighbors, the finite volume method is to integrate the conservation equation over the finite volume ΔV. After the Gauss theorem is applied, one can obtain a flux balance equation over the cell. For example, for a cell P shown in Fig. 1(b), the flux balance can be written as

$$\left(a_\varphi \frac{\partial \varphi}{\partial t} \right)_P \Delta V + \sum_{f=1}^{N_f} b_\varphi \varphi_f \mathbf{v}_f \cdot \mathbf{S}_f = \sum_{f=1}^{N_f} \Gamma_{\varphi_f} \nabla \varphi_f \cdot \mathbf{S}_f + B_\varphi \Delta V, \tag{7}$$

where P denotes the nodal point at the cell center and f is the midlocation of the cell face, $\mathbf{S}_f$ is the surface vector of the face f. The number of faces N_f of each cell is different and depends on the refinement or coarsening. The calculation of the cell value is simply by distance-weighted interpolation. However, care must be taken for the diffusion term, because we do not want the vertex points to be involved, which may complicate the coding. To do so, the approximation proposed by Mathur and Murthy [16] is adopted. Talking the face f in Fig. 1(b) as an example,

$$\nabla \varphi \cdot \mathbf{S}_f = \frac{\varphi_{Nb} - \varphi_P}{L_{PNb}} \frac{\mathbf{S}_f \cdot \mathbf{S}_f}{\mathbf{S}_f \cdot \mathbf{e}_\xi} + (\nabla \varphi)_f \cdot \left(\mathbf{S}_f - \mathbf{e}_\xi \frac{\mathbf{S}_f \cdot \mathbf{S}_f}{\mathbf{S}_f \cdot \mathbf{e}_\xi} \right), \tag{8}$$

where $\mathbf{e}_s$ and $\mathbf{e}_\xi$ are unit vectors shown in Fig. 1(b). Although the above approximation does not require the vertex values, the approximation of the gradient at the cell face [i.e., $(\nabla \varphi)_f$] is necessary. Two approaches can be used. One is to evaluate the value at the cell center of the related cells and then the face value can be interpolated linearly from its adjacent cells. The other way is to find the best fit through least squares from the neighbor cells [17]. Both approaches work well, but the former takes less effort in computation. Further approximation for the time derivative is necessary and the implicit Euler scheme is adopted. Although a higher-order scheme can be used, it needs more memory and computation at each time step. Moreover, in the simulation of dendritic growth, the refined zone is very thin. Hence, the time step is restricted by the amount of interface movement such that the advancement of the new interface needs to be inside the zone. Therefore, since time step is small, the first-order Euler scheme is adequate. After assembling the flux balance equations for all cells and imposing the boundary conditions for the boundary cells, one can solve the nonlinear algebraic equations (for each time step) easily. Due to the incompress-

TABLE I. The corresponding coefficients for different conservation variables.

φ	a_φ	b_φ	Γ_φ	B_φ
1	0	1	0	0
$\boldsymbol{\nu}$	$1/D$	1	Pr	$-\nabla P + \mathbf{F}$
θ	1	D	D	$\frac{1}{2}\frac{\partial \phi}{\partial t}$
ϕ	$A(\mathbf{n})^2$	0	$A(\mathbf{n})^2$	$[\phi - \lambda\theta(1-\phi^2)](1-\phi^2) + \frac{\partial}{\partial x}\left(\lvert\nabla\phi\rvert^2 A(\mathbf{n}) \frac{\partial A(\mathbf{n})}{\partial \phi_x} \right) + \frac{\partial}{\partial y}\left(\lvert\nabla\phi\rvert^2 A(\mathbf{n}) \frac{\partial A(\mathbf{n})}{\partial \phi_y} \right)$

TABLE II. Comparison of different methods for estimating the local tip radius.

	Eq. (12)		Second-order fitting		Fourth-order fitting	
$\Delta x_{\min}(w_0)$	$R(w_0)$	Error (%)	$R(w_0)$	Error (%)	$R(w_0)$	Error (%)
0.4	1.78	71.65	1.62	49.58	1.2485	37.26
0.2	1.37	32.11	1.29	19.11	1.07	17.97
0.1	1.12	8.00	1.135	4.801	0.948	4.520
R_{ext}	1.037		1.083		0.907	

ibility of the melt, the pressure does not appear explicitly in the equation of continuity, i.e., Eq. (4). An iteration scheme for the velocity/pressure coupling is also required. The SIMPLE scheme [18] and momentum interpolation [19] are further adopted. In addition, the Gauss-Siedel method is used for inner iterations (linearized equations) for all variables. We have also used the ILU(0)-preconditioned GMRES method [15], but the overall performance has not improved much.

The simulation starts from a small seed with an artificial hyperbolic tangent function for temperature and the phase-field variable:

$$\begin{aligned} \theta &= 0, \quad |x| < R_0, \\ \theta &= \Delta(1 - e^{-(|x|-R_0)}), \quad |x| \geqslant R_0, \\ \phi &= -\tanh[(|\mathbf{x}| - R_0)/\sqrt{2}], \end{aligned} \tag{9}$$

where R_0 is the initial radius of the seed. Furthermore, the velocity at the inlet is set to be uniform at U. The outflow boundary conditions also need to stratify the overall flow continuity. In addition, the side boundary is assumed to be far enough, so that zero gradient of the velocity, or the stress-free condition, is imposed.

Before presenting the results for comparison with the theory, we have defined the growth Peclet number $P_c = VR/2D$, where R is the tip radius. Similarly, the flow Peclet number is defined as $P_f = UR/2D$. Based on these two dimensionless numbers, the Oseen-Ivantsov solution obtained by Bouissou and Pelce [4] for a parabolic dendrite can be represented as the following:

$$\Delta = P_c \exp(P_c - P_f) \times \int_1^\infty \frac{\exp\left\{ -P_c \eta + P_f \left(2 + \int_1^\eta [g(\varsigma)/\sqrt{\varsigma}] d\varsigma - \eta \right) \right\}}{\sqrt{\eta}} d\eta. \tag{10}$$

where

$$g(\varsigma) = \frac{\sqrt{\varsigma}\,\mathrm{erfc}(\sqrt{\mathrm{Re}\,\varsigma/2}) + \sqrt{2/(\pi\,\mathrm{Re})}[\exp(-\mathrm{Re}/2) - \exp(-\mathrm{Re}\,\varsigma/2)]}{\mathrm{erfc}(\sqrt{\mathrm{Re}/2})}.$$

Also, the Reynold number is defined as $\mathrm{Re} = UR/\nu = 2P_f \mathrm{Pr}$, where ν is the kinematic viscosity, erfc is the complementary error function. For diffusive growth $P_f = 0$ and Eq. (10) can be reduced to the Ivantsov solution

$$\Delta = \sqrt{P_c} e^{P_c} \int_{P_c}^\infty \frac{e^{-t}}{\sqrt{t}} dt = \sqrt{\pi P_c} e^{P_c} \mathrm{erfc}(\sqrt{P_c}). \tag{11}$$

For a given supercooling, one can calculate the Peclet number P_c. If the tip radius R is known, the tip speed can be calculated. However, the question left over is how to estimate the tip radius and where does the tip radius need to be used for the comparison with the theory. Because the previous solutions neglect the interfacial energy, the local tip radius may not be a right value to use. Indeed, in a recent calculation by Tong, Beckermann, and Karma [9], they showed that a good agreement of their phase-field simulation with Eq. (10) was obtained at a high supercooling ($\Delta = -0.55$), but only when the tip radius was obtained by a parabolic fitting of the overall dendrite head. In addition, to be more convincing, we have also performed an extensive comparison of several ways for estimating the local tip radius. Interestingly, we have found that the local radius is very sensitive to the mesh used, especially at high supercoolings [21]. For the present scheme, the local curvature can be calculated at the cell P having $\phi = 0$ at the tip as follows:

$$\begin{aligned} \kappa_P &= \frac{1}{\Delta V} \int \kappa \, dV = \frac{-1}{\Delta V} \int \nabla \cdot \left(\frac{\nabla \phi}{|\nabla \phi|} \right) dV \\ &= \frac{-1}{\Delta V} \oint \left(\frac{\nabla \phi}{|\nabla \phi|} \right) \cdot \mathbf{n} dS \cong \frac{-1}{\Delta V} \sum_{f=1}^{N_f} \left(\frac{\nabla \phi}{|\nabla \phi|} \right)_f \cdot \mathbf{n}_f \Delta S. \end{aligned} \tag{12}$$

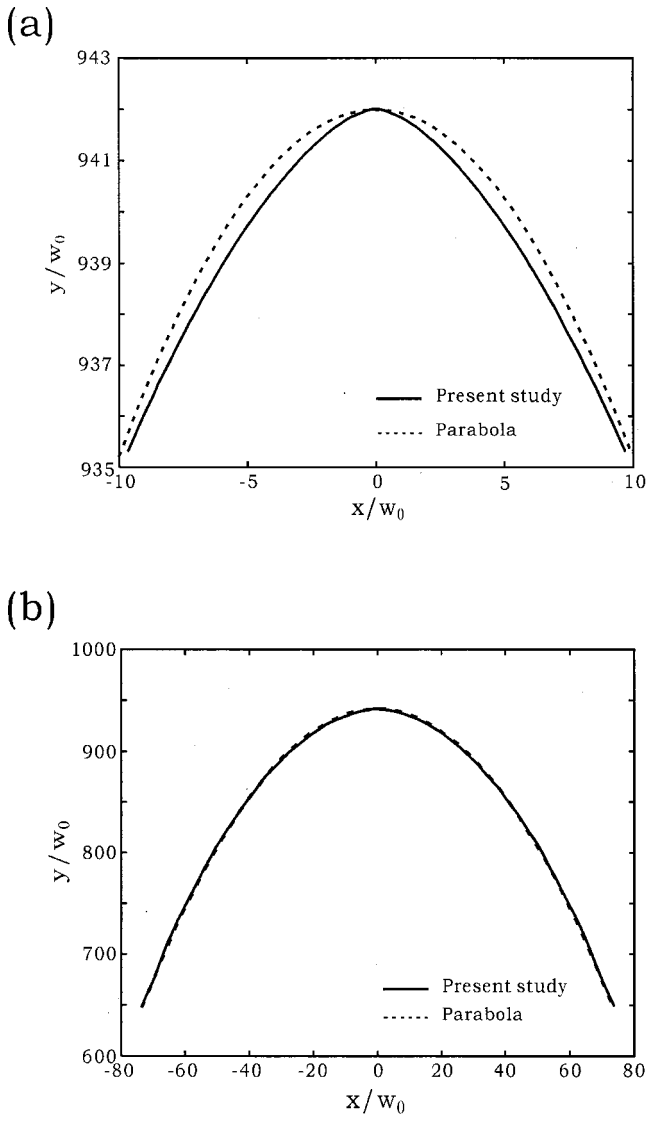

FIG. 2. (a) The local tip shape and the best-fitting parabola, (b) the overall tip and the best-fitting parabola, $\Delta=-0.55$ and $U=0$.

The tip radius $R=1/\kappa_P$. Because the exact position of $\phi=0$ may not be right at the cell center, the above approximation, which is based on the mean-value theory, has an error of the order of the cell size. In other words, it is expected to have only first-order accuracy. Another way for estimating the local tip radius is by using a polynomial fitting (up to second or fourth orders), i.e., $y(x)=ax^4+bx^2+c$, $\kappa(x)=|y''|/(1+y'^{3/2})$, where $y''=\partial^2 y/\partial x^2$ and $y'=\partial y/\partial x$. Still, the tip shape is obtained by interpolation from the phase field at $\phi=0$ and the error depends on the interpolation error as well. For a parabolic shape, the radius of curvature is constant everywhere. The results of the calculated tip radius by different approaches for $\Delta=-0.55$ are shown in Table II, where R_{ext} is obtained by Richardson extrapolation from the finest two grids; the calculation by Eq. (12) has only first-order accuracy; in fact, the convergence order obtained from the calculations is found to be better, being about 1.5. As shown, when $\Delta x_{\min}$ is not much smaller than the local radius, an accurate estimation by Eq. (12) is not possible. On the other hand, if the cell size is reduced, the accuracy is greatly improved. However, the computational cost increases as well. From Table II, it is clear that the higher-order estimation through polynomial fitting gives a better result. Nevertheless, although the minimum cell size is found adequate for the phase-field simulation [5,9], the estimation of the local tip radius may still be erroneous. In addition, as shown in Fig. 2(a), the tip does not fit locally to a parabola nicely due to the effect of interfacial energy [6]. On the contrary, the overall shape of the dendrite can be fitted nicely, as shown in Fig. 2(b), by a parabola. More importantly, this overall tip radius, which is constant everywhere, is not sensitive to the mesh size.

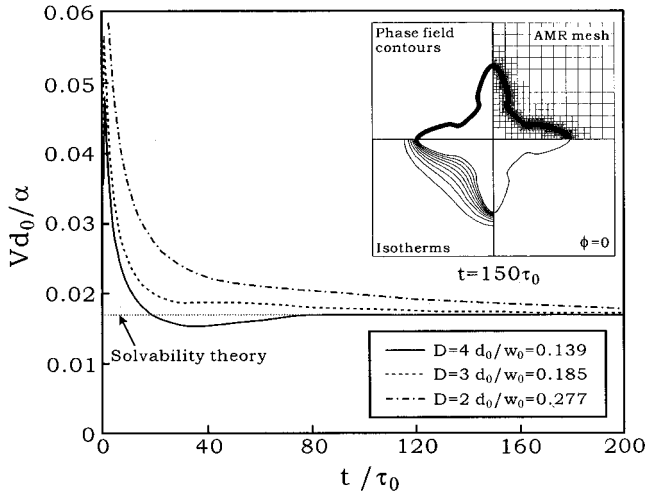

FIG. 3. Calculated tip speed at various parameters. The mesh and the phase and thermal fields (size: $-128w_0<x<128w_0$; $-128w_0<y<128w_0$) are also illustrated for $t=150\tau_0$. In all cases, the solvability limit can be approached easily.

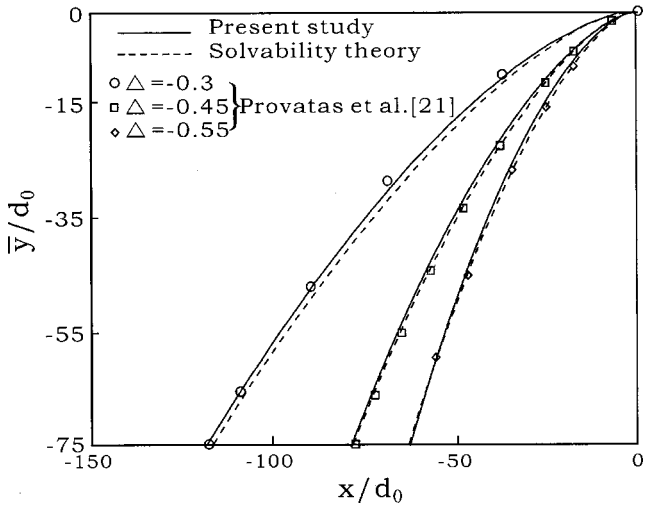

FIG. 4. Calculated local tip shapes for different supercoolings at $U=0$; $\bar{y}=y-y_{\text{tip}}$; y_{tip} is the y coordinate of the tip.

TABLE III. Comparison for diffusive growth at high supercooling ($\varepsilon = 0.05$).

Δ	d_0/w_0	D	$L_D(w_0)$	Level	$\Delta x_{\min}(w_0)$	Theoretical tip speed	Karma and Rappel [5]	Present	Error (%)
−0.55	0.139	4	128	6	0.4	0.017 0	0.017 4	0.001 71	0.6
−0.55	0.185	3	1024	9	0.4	0.017 0	0.001 75	0.001 69	0.6
−0.55	0.277	2	1024	9	0.4	0.017 0	0.001 68	0.001 67	1.2
−0.50	0.185	3	256	7	0.4	0.009 85	0.010 05	0.009 87	0.2
−0.45	0.139	4	1024	9	0.4	0.005 45	0.005 40	0.005 41	1.1
−0.45	0.185	3	1024	9	0.4	0.005 45	0.005 57	0.005 40	0.9
−0.30	0.055	10	1000	8	0.52	0.000 68	0.000 64	0.000 664	3.75

IV. RESULTS AND DISCUSSION

A. Benchmark comparison for diffusive growth

Before presenting the results for convective growth, we have to make sure that the calculations for diffusive growth are consistent with previous studies. For high supercoolings, Karma and Rappel [5] have presented detailed benchmarking, and their results agree very well with the prediction of the solvability theory. Therefore, we have repeated the same calculations for $\Delta = -0.55$ first. Figure 3 shows the evolution of the tip speed; the dendrite shape (phase-field variable), isotherms, and mesh at $t = 150\tau_0$ are also illustrated. In this case, only six levels of meshes are used in the AMR. As shown in Fig. 3, the tip speed reaches a steady state quickly for three different parameters. Interestingly, due to the fast growth rate, the growth of each arm is quite independent of the other. Also, the domain size has very little effect on the result. Further comparisons can be found in Table III, where different parameters and domain sizes are also used for comparison. As shown, good agreement is found. Moreover, the tip shapes at various supercoolings are compared with previous results in Fig. 4. Again, good agreement is obtained.

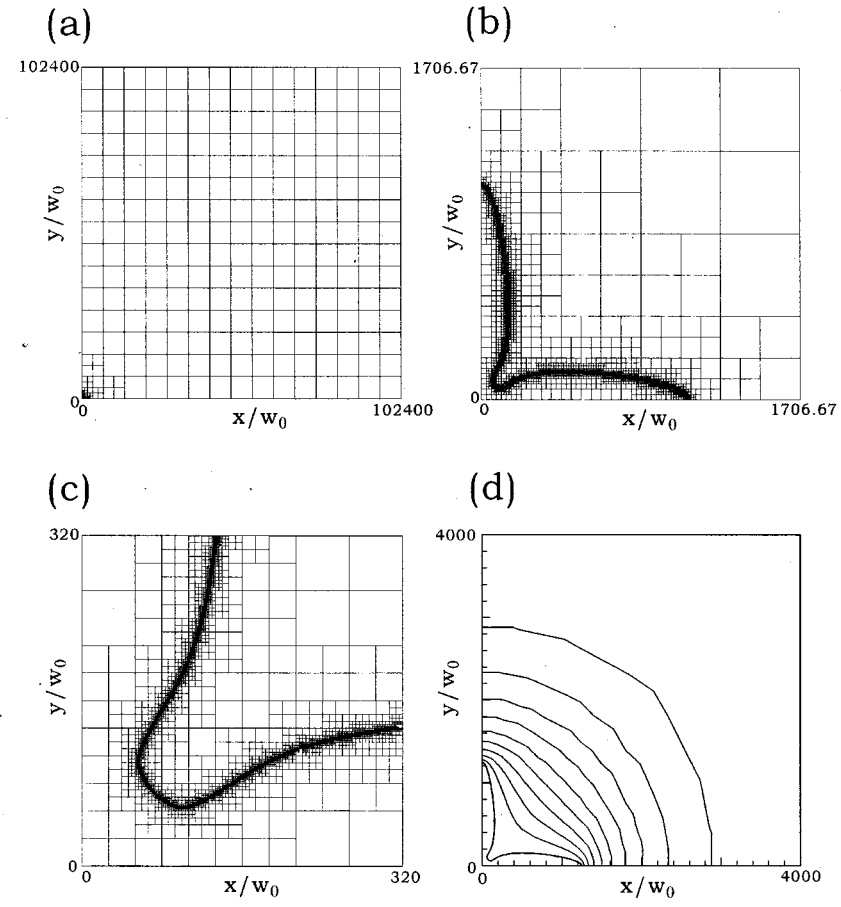

FIG. 5. Mesh for $\Delta = -0.25$ ($U = 0$) at different length scales: (a) the full domain, (b) domain for the dendrite only, (c) a local view of the mesh, (d) the isotherms around the dendrite.

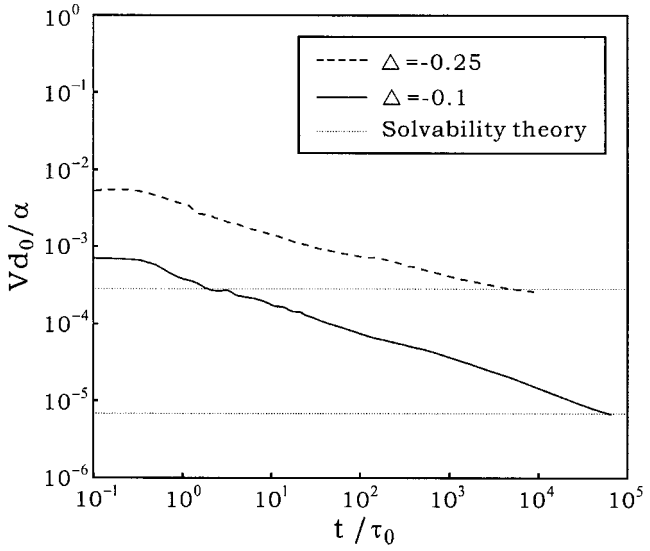

FIG. 6. Evolution of dimensionless tip speed at $\Delta=-0.25$ and -0.1.

More importantly, as mentioned previously, the overall dendrite shapes remain parabolic, even though the local dendrite shape deviates from the analytical shape slightly due to the interfacial energy.

The present AMR scheme is particularly efficient in the phase-field simulation. For a uniform mesh, if the domain size is L_D and the minimum cell size $\Delta x_{\min}$, the total cell number is $(L_D/\Delta x_{\min})^2$. Then, for a given tip growth rate V and time step τ_0, one needs $L_D/(V\tau_0)$ time steps to grow a dendrite to the size of the domain. Then, if the solution time at each step is about to be the same, the total CPU time for a calculation using a uniform mesh becomes

$$(\text{CPU time})^{\text{uniform}} \propto \frac{L_D}{V\tau_0}\left(\frac{L_D}{\Delta x_{\min}}\right)^2=\left[\frac{1}{V\Delta x_{\min}^2\tau_0}\right]{L_D}^3.$$

However, for an AMR scheme, if most of the fine cells are used to describe the thermal boundary layer (thickness δ) near the interface, the cell number required is about $\delta L_D/\Delta x_{\min}^2$; $\delta\sim\alpha/V$. Again, for the same number of time steps $L_D/(V\tau_0)$, the CPU time for a calculation using ARM is only about

$$(\text{CPU time})^{\text{AMR}} \sim \frac{L_D}{V\tau_0}\left(\frac{\delta L_D}{\Delta x_{\min}}\right)^2=\left[\frac{\alpha}{V^2\Delta x_{\min}^2\tau_0}\right]{L_D}^2.$$

Therefore, when the calculation domain is increased, an AMR scheme is much more efficient. In our scheme, the CPU time is scaled by about $L_D^{2.1}$. The calculation using an explicit scheme for time integration does not reduce the overall CPU time much, as compared with the implicit scheme, because the largest time step is limited by the Courant-Friedricks-Lewey condition. For the implicit scheme used here, although each time step requires more CPU time for the solution of nonlinear equations, the time step allowed can be much larger. Nevertheless, the largest time step is still restricted by the thickness of the refined zone. If the new interface is beyond the refined zone, significant numerical noises are introduced.

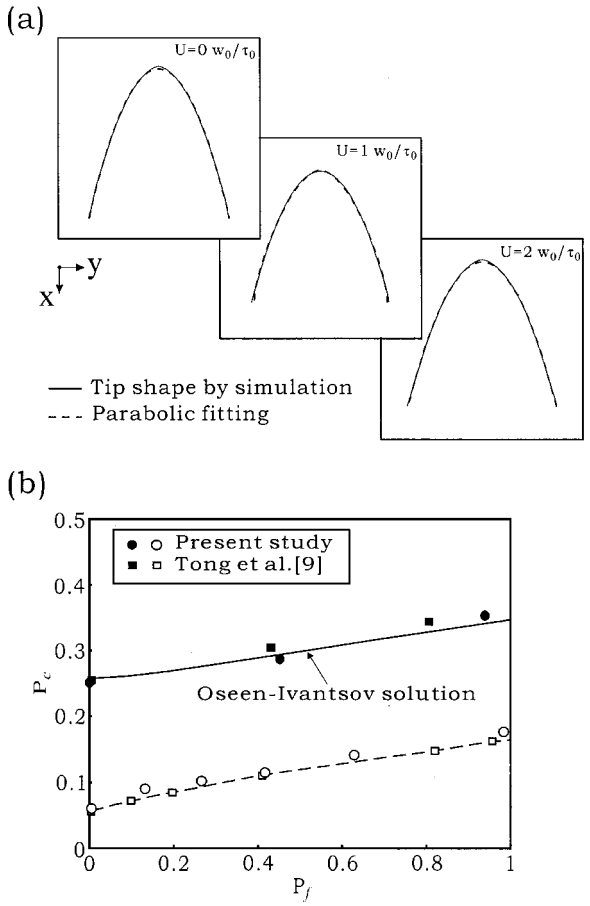

FIG. 7. The effect of flow on the dendrite shape and tip speed, (a) overall dendrite head: from the left to the right the figure size is $-85w_0<x<-40w_0; -25w_0<y<25w_0$, $-477.5w_0<x<-437.5w_0; -25w_0<y<25w_0$, and $(-2005w_0<x<-1965w_0; -20w_0<y<20w_0)$, respectively. (b) The effect of flow Péclet number; the dashed line in (a) is the best-fitted parabola, in (b) the opened symbols are the results using the local tip radius.

The benchmark comparison for low supercoolings is much more difficult. Unlike that at high supercoolings, the growth is much slower at low supercoolings. Hence, the time to reach a steady state is also much longer. Furthermore, due to the thermal diffusion of the side arms, the tip speed may not converge to the solvability limit [6]. Indeed, in order to prevent the far field boundary from being affected, the domain size needs to be much larger. Provatas, Goldenfield, and Dantzig [6] proposed heuristic criteria: the domain size required is about $(5-10)D/V$ and the time for reaching a steady state is estimated to be D/V^2. For $\Delta=-0.1$, the domain size required is about $102\,400\times102\,400(\Delta x_{\min})^2$, while the minimum cell size is about $0.833w_0$. Moreover, the time for reaching a steady state is longer than $10^6\tau_0$. Figure 5 shows the meshes at different view scales and the calculated isotherms at $t=60\,000\tau_0$ [Fig. 5(d)]. As shown, unlike that in Fig. 3, the isotherms are much more diffusive. The calculated tip speeds at $\Delta=-0.1$ and -0.25 are shown in Fig. 6, respectively; we have purposely presented them in a log-log

scale in order to see the asymptotic decay rate at longer time. As shown, for both cases, the growth rate is slightly lower than the prediction of the solvability theory at a longer time. It is realizable that due to the growth of side arms the growth environment is getting warmer as compared with that of a single arm, which is assumed in theory. Accordingly, the growth rate is reduced. These results slightly differ from those by Provatas, Goldenfield, and Dantzig [6].

B. Effects of forced flow at $\Delta=-0.55$

Recently, Tong, Beckermann, and Karma [9] performed elegant calculations to study the effects of a forced flow on the selection of tip shape and velocity. Their results agree quite well with the Oseen-Ivantsov solution if the tip radius is estimated by a parabolic fitting to the overall dendrite head. We have also performed the same calculations using the AMR scheme. The comparison is shown in Fig. 7. In Fig. 7(a), we again illustrate the suitability of using a parabola to fit the upstream dendrite head grown at different flow rates. As shown, beside a small area at the tip, the overall dendrite head can be represented by a simple parabola very well. The comparison with the Oseen-Ivantsov solution and the previous calculations [9] is further illustrated in Fig. 7(b), where the results (open symbols) using the local tip radius (second-order fitting) for the Peclet numbers are included. As shown, good agreement with the theory (solid line) is found when the overall tip radius is used. Nevertheless, we have further examined the effects of domain size for $U=w_0/\tau_0$, and the results are summarized in Table IV. As shown, our converged velocity is slightly lower than that obtained by Tong, Beckermann, and Karma [9], where the largest domain size used by them was $1024\times2048(\Delta x_{\min})^2$, or the total number of cells number were 1024×2048. As shown in Table IV, increasing the domain size slightly reduces the tip velocity. For the domain size up to $2048\times4096(\Delta x_{\min})^2$, being more than ten times the dendrite size, the effect of domain size can be neglected. However, if the domain is small, the fluid flow boundary condition at the boundary is affected. In other words, even at high supercooling, the domain size cannot be too small, e.g., $256\times512(\Delta x_{\min})^2$, for convective growth, even though it is enough for diffusive growth. It is particularly true for the materials studied here (succinonitrile) that the kinematic viscosity is much larger than the thermal diffusivity ($\mathrm{Pr}=\nu_m/\alpha_m=23.1$); here, the momentum boundary layer is thicker than the thermal one.

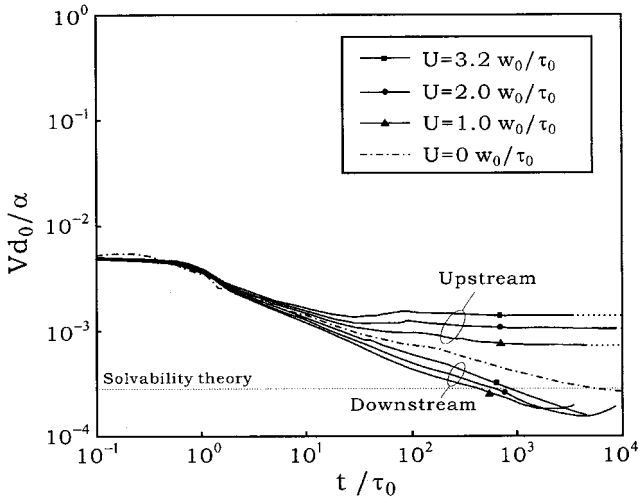

FIG. 8. Effects of flow velocity on the upstream and downstream tip speeds, $\Delta=-0.25$.

C. Effects of forced flow at low supercoolings

The growth behavior for diffusive growth, such as that in Fig. 6, is typical for low supercoolings. This is due to the much lower growth rate and the thicker thermal boundary layer. As a result, the comparison of the simulation with the theory becomes difficult. In addition, as just mentioned, the interaction of side arms makes the comparison even more difficult. For diffusive growth, a simple way for comparison is to reduce the side-arm effect by reducing the domain size in the side-arm direction [6]. This also reduces the warming effect from the side arm (releasing the heat of fusion during growth). Even so, as shown by Provatas, Goldenfield, and Dantzig [6], some discrepancy with the theory still exists.

Interestingly, once the tip velocity is enhanced by the flow, we find that the tip velocity reaches a steady state more quickly and the upstream tip growth becomes similar to the case at high supercooling. As shown in Fig. 8, for $\Delta=-0.25$, with a forced flow, the growth velocity of the up-

TABLE IV. Effect of domain size for convective growth ($\Delta=-0.55$).

Domain size	Initial CV's	Level	$\Delta x_{\min}$	Vd_0/α[a]	No. of CV's ($t=100\tau_0$)
256×128	20×10	6	0.4	0.0260	6256
512×256	20×10	7	0.4	0.0232	6187
1024×512	20×10	8	0.4	0.0224	6240
2048×1024	20×10	9	0.4	0.0224	6223
4096×2048	20×10	10	0.4	0.0223	6215
512×256	40×20	6	0.4	0.0231	6823
1024×512	80×40	6	0.4	0.0224	9335
2048×1024	160×80	6	0.4	0.0224	19 159
2048×1024	20×10	10	0.2	0.0226	21 991
4096×2048	20×10	11	0.2	0.0227	22 011

[a]Upstream tip velocity of Tong, Beckermann, and Karma of 0.0240.

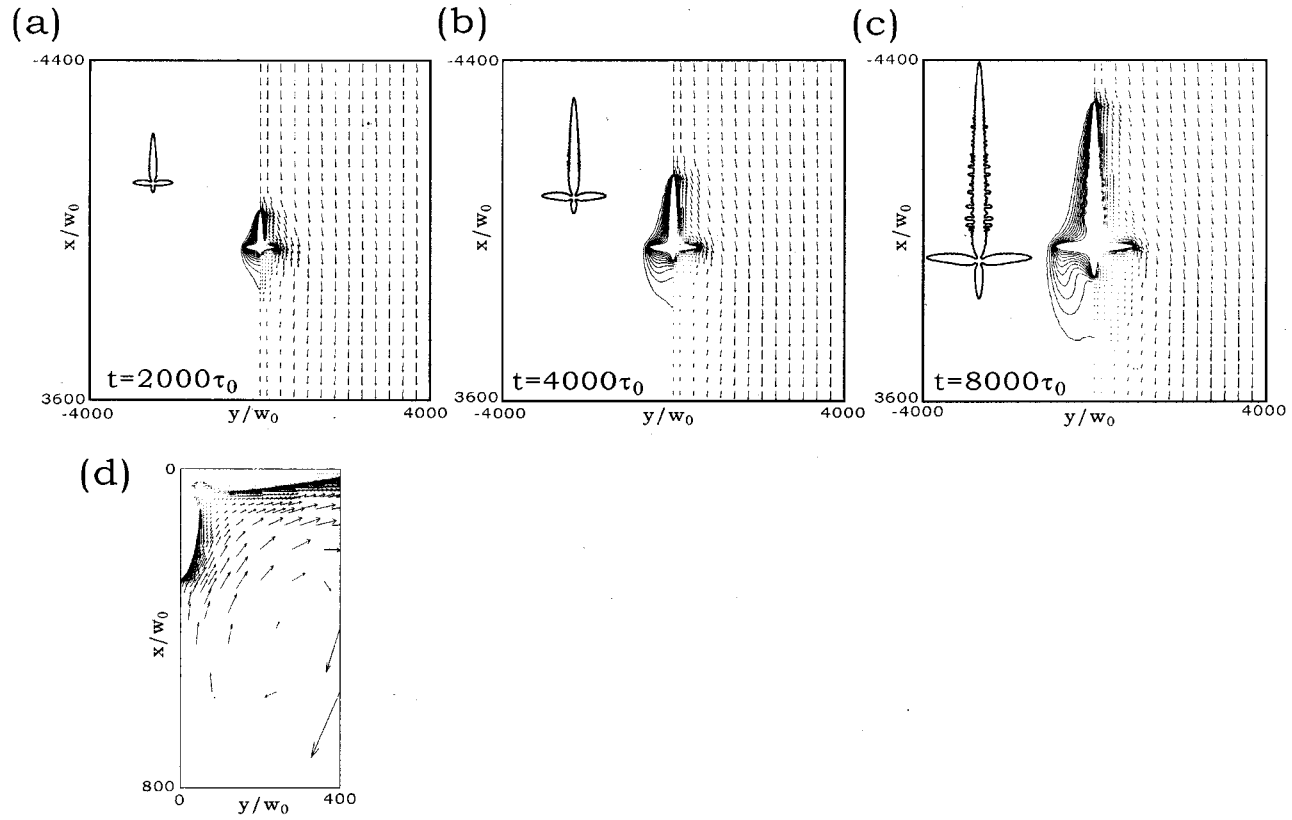

FIG. 9. Calculated flow and thermal fields and the dendrite shapes at different times: (a) $t=2000\tau_0$, (b) $t=4000\tau_0$, (c) $8000\tau_0$, (d) a local view of the back flow of (b), $\Delta=-0.25$ and $U=2w_0/\tau_0$.

stream tip approaches a steady state quickly; that for diffusive growth (or $U=0$) is put together for comparison. The downstream arm grows slower, but the growth rate bounds back after a longer time. Selected flow and temperature fields for $U=2w_0/\tau_0$ at different times are shown in Fig. 9. As shown, at the upstream, due to the flow, the thermal boundary layer is much thinner at the tip front. As a result, the growth is faster there, as shown in Fig. 8. Due to the fast growth, the growth reaches a steady state quickly. More importantly, as shown in Fig. 9, the isotherms are pushed toward the side arms. Accordingly, the thermal influence from the side arms is suppressed. In other words, the upstream dendrite grows like a single one.

In addition, as shown in the lower part of Fig. 8, the downstream arm shows some abnormal growth behavior. As shown, when the convection is strong, the downstream tip growth is getting slower at the beginning. However, at a longer time, the velocity reaches a minimum and then starts to increase. We examine the local flow field near the downstream in Fig. 9. At the beginning, there is no clear vortex [Fig. 9(a)]. However, after the boundary separation at a longer time [Figs. 9(b) and 9(c)], there is a wake behind the side arms as shown in Fig. 9(d), which is a local view of Fig. 9(c). Because the back flow increases, the isotherms are pushed toward the downstream tip. Hence, the local growth rate is enhanced.

Notably, as shown by the upstream arm, many side branches are induced, while other arms remain smooth. This is believed to be the cause of noises (likely to be numerical) that are amplified by the flow. For a purely diffusive growth at the same supercooling or lower, the same mesh does not induce any side branches along the arms at all. The side branching increases with the increasing flow velocity and decreasing supercooling. Further refining the mesh delays slightly the onset of the side branching. In reality, the side branching due to the flow is typical [20] and it may be due to thermal noises. However, from the stability point of view, it is believed that the branching state is more stable than the smooth one. Therefore, the branching shown in Fig. 9 is believed to be physical.

If we further convert the steady growth velocities and the tip radii (using one half of the arm) into the growth Peclet number as a function of the flow Peclet number, the comparison with the Oseen-Ivantsov solution is shown in Fig. 10. As shown, the agreement is quite satisfactory. Nevertheless, the calculated Peclet numbers are slightly lower than the analytical ones.

The calculation for $\Delta=-0.1$ show similar results [22], but the side branching becomes much more significant. The comparison with the Oseen-Ivantsov solution is shown in Fig. 11. Again, the agreement is satisfactory. The calculated growth P_c's are slightly lower than the analytical ones. Now, the question left over is whether or not the dendrite arm still remains parabolic. Indeed, we have found a positive sign from the comparison with the Oseen-Ivantsov solution, which assumes a parabolic dendrite shape, even though there are many side branches along the arm. To further illustrate that, we have performed a simple self-affine transformation

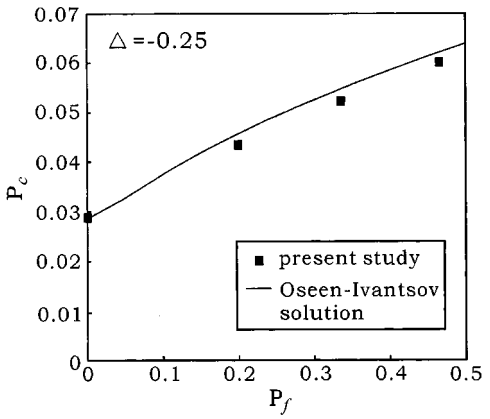

FIG. 10. The effect of flow Péclet number P_f on the growth Peclet number P_c for $\Delta=-0.25$.

by scaling x using $(x-x_b)/x_{\max}$ and y using $y/y_{\max}$ for the steady-state arm shape at different growth periods ranging from $2000\tau_0$ to $8000\tau_0$; x_b is the base position, $x_{\max}$ the maximum arm length, and $y_{\max}$ the dendrite width by ignoring the side branches. For $\Delta=-0.25$, as shown in Fig. 12(a) the rescaled shape remains to be parabolic and the shape seems to be universal. Beside the side branches, the overall shape is almost the same as the diffusive one, as shown in Fig. 12(b). In other words, the self-affine shape is not affected much by the flow. Interestingly, it is affected very little by the supercooling as well [22]. For a steady growth, with or without the flow, if $x_{\max}$ is proportional to t^{β} and $y_{\max}$ to t^{η}, then the best fitting gives $\beta\sim 1$ and $\eta\sim 0.5$, as shown in Table V. This scaling result can be easily understood. Since both the velocity $V_t\sim dx/dt\sim \beta t^{\beta-1}$ and the radius of curvature $R\sim(d^2x/dy^2)^{-1}\sim t^{2\eta-\beta}$ are constant at steady state, one shall get $\beta=1$ and $\eta=0.5$. The exponents further indicate clearly that the overall tip shape continues to be parabolic, even though the local tip is not. In other words, because the tip head continues to be parabolic, the results thus agree reasonably well with the Oseen-Ivantsov solution.

V. CONCLUSIONS

An efficient adaptive finite volume method is developed for the phase-field simulation of dendritic growth in a forced flow at various supercoolings for Pr=23.1. The scheme is efficient in that the computational time is proportional to the domain size. The calculations for high supercooling ($\Delta=-0.55$) agree very well with previous calculations and

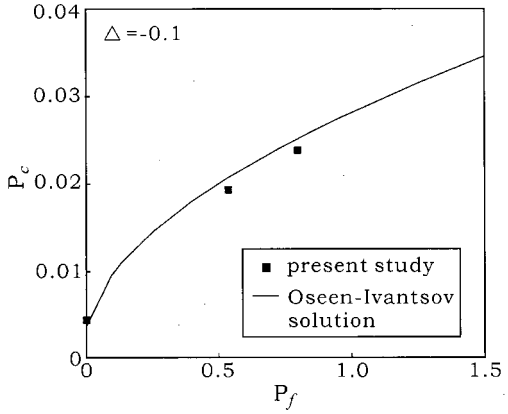

FIG. 11. The effect of flow Péclet number P_f on the growth Péclet number P_c for $\Delta=-0.1$.

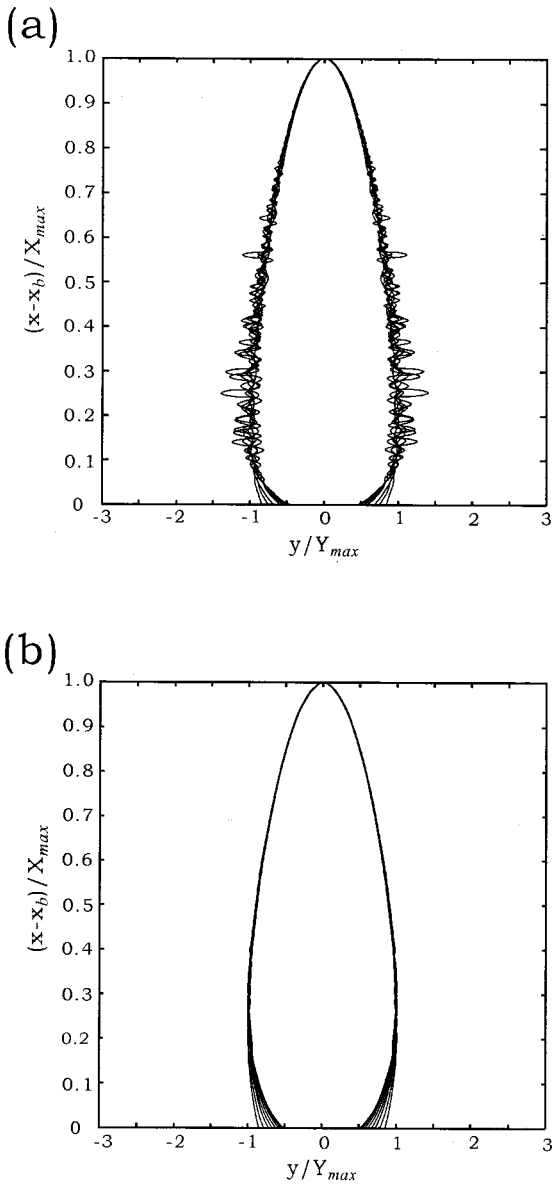

FIG. 12. Self-affine shapes: (a) $U=1w_0/\tau_0$, (b) $U=0$, nine shapes from $t=2000\tau_0$ to $8000\tau_0$ are used, $\Delta=-0.25$.

TABLE V. Self-affine parameters β and η in different supercoolings and flow rates.

Δ	$U(w_0/\tau_0)$	β	η
−0.25	1	1.0828	0.4410
	2	1.0693	0.5065
	3.2	1.0904	0.5210
−0.1	5	1.0698	0.5445
	10	1.058	0.4452

theory if the upstream tip radius is obtained from the overall dendrite head at the upstream. Even with high supercooling, we find that the domain size cannot be too small because the far field flow boundary can be easily affected due to the thicker momentum boundary layer from the dendrite. As a result, the domain size required for this is much larger than that for diffusive growth.

For low supercoolings, without convection, our results agree reasonably well with previous calculations. Due to the small tip velocity, it takes a long time to reach a steady state. Therefore, the domain size needs to be extremely large to avoid the far field from being affected. Although for such a large domain, while keeping very small cells at the interface, the calculation is difficult to be carried out by a structured mesh, it can be easily be resolved by the present adaptive scheme. Even so, the time for reaching a steady state for the tip speed is extremely long. However, with a forced flow, the upstream tip speed is enhanced. As a result, the upstream tip can reach a steady state quickly. More importantly, due to the flow, the thermal effect of the side arms is suppressed. As a result, we have found that the calculated results agree well with the Oseen-Ivantsov solution. Side branches along the upstream are induced easily with the increasing flow and decreasing supercooling. Nevertheless, the overall arm shape continues to be parabolic and is not affected much by the flow. As a result, at steady state, the upstream arm shape continues to have a self-affine nature.

ACKNOWLEDGMENTS

C.W.L would like thank Professor R. F. Sakerka for introducing this topic and for valuable discussions. Fruitful discussions with Professor Amberg at the beginning of this study are also appreciated. This research was sponsored by the National Science Council of the Republic of China.

[1] G. P. Ivantsov, Dokl. Akad. Nauk SSSR **558**, 576 (1947).
[2] J. S. Langer, in *Chance and Matter*, Proceedings of the Les Houches Summer School, Session XLVI, edited by J. Souletie, J. Vannimenus, and R. Stora (North-Holland, Amsterdam, 1987), pp. 629–711.
[3] D. Kessler, J. Koplik, and H. Levine, Adv. Phys. **37**, 255 (1988).
[4] Ph. Bouissou and P. Pelce, Phys. Rev. A **40**, 6673 (1989).
[5] A. Karma and W. J. Rappel, Phys. Rev. E **53**, R3017 (1996); **57**, 4323 (1998).
[6] N. Provatas, N. Goldenfield, and J. Dantzig, Phys. Rev. Lett. **80**, 3308 (1998).
[7] A. Karma and W. J. Rappel, Phys. Rev. Lett. **77**, 4050 (1996).
[8] A. Karma and W. J. Rappel, Phys. Rev. E **53**, R3017 (1996).
[9] X. Tong, C. Beckermann, and A. Karma, Phys. Rev. E **61**, 49 (2000).
[10] Ph. Bouissou, P. Pelce, and P. Tabeling, Phys. Rev. A **40**, 509 (1989).
[11] V. Emsellem and P. Tabeling, J. Cryst. Growth **156**, 285 (1995).
[12] Y. W. Lee, R. Ananth, and W. N. Gill, J. Cryst. Growth **132**, 226 (1993).
[13] R. Tonhardt and G. Amberg, J. Cryst. Growth **213**, 161 (2000).
[14] C. Beckermann, H.-J. Diepers, I. Steinbach, A. Karma, and X. Tong, J. Comput. Phys. **154**, 468 (1999).
[15] C. W. Lan, C. C. Liu, and C. M. Hsu, J. Comput. Phys. (to be published).
[16] S. R. Mathur and J. Y. Murthy, Numer. Heat Transfer, Part B **31**, 195 (1996).
[17] S. Muzaferija and D. Gosman, J. Comput. Phys. **138**, 766 (1997).
[18] S. V. Patankar, *Numerical Heat Transfer and Fluid Flow* (Hemisphere, Washington, D.C., 1980).
[19] C. M. Rhie and W. L. Chow, AIAA J. **21**, 1527 (1983).
[20] N. Noel, H. Jamgotchian, and B. Billia, J. Cryst. Growth **181**, 117 (1997).
[21] Provatas, N. Goldenfeld, and J. Dantzig, J. Comput. Phys. **148**, 265 (1999).
[22] C. W. Lan, C. M. Hsu, and C. C. Liu, J. Cryst. Growth (to be published).